Metals

Microstructure and mechanical properties of high-strength steel welding consumables with a minimum yield strength of 1100 MPa

Phillip Haslberger[1,*] iD, Sylvia Holly[2,3], Wolfgang Ernst[4], and Ronald Schnitzer[1]

[1] *Department of Physical Metallurgy and Materials Testing, Montanuniversität Leoben, Franz-Josef-Straße 18, 8700 Leoben, Austria*
[2] *voestalpine Boehler Welding Austria GmbH, Kapfenberg, Austria*
[3] *Present address: voestalpine Wire Technology GmbH, Bruck/Mur, Austria*
[4] *voestalpine Stahl GmbH, Linz, Austria*

ABSTRACT

Welded high-strength steel components have great potential for use in lightweight constructions or highly loaded structures. Welding of steels with a yield strength of more than 1100 MPa is particularly challenging because of the toughness requirements for the weld metal. Currently, a new generation of welding consumables with a minimum yield strength of 1100 MPa has been developed. Based on electron backscatter diffraction and atom probe tomography, a concept for toughening and strengthening of all-weld metal samples was deployed. Starting from a martensitic all-weld metal sample with an approximate yield strength of 1000 MPa, a reduction in manganese and silicon content resulted in a refined microstructure with a lower prior austenite grain size and effective grain size. Furthermore, a higher average grain boundary misorientation was measured, which influences the toughness positively. An addition of vanadium caused the formation of vanadium-rich clusters, which increased the strength of the all-weld metal significantly. With a combination of these two mechanisms, it was possible to produce an all-weld metal sample with the required yield strength of more than 1100 MPa and an acceptable toughness.

Introduction

In lightweight constructions and for highly loaded components, high-strength steels are frequently used. Welding plays a crucial role in manufacturing of these constructions. Due to the high demand, a variety of steels with a strength in the range of 1000–1300 MPa is currently available. However, gas metal arc welding and other modern welding techniques require the use of a suitable filler material. Although it was shown that undermatching welding consumables can be sufficient for some welding processes and conditions [1–3], a new generation of welding consumables with a higher strength level is

Address correspondence to E-mail: phillip.haslberger@unileoben.ac.at

desirable, while keeping the toughness above 47 J at − 20 °C.

Recently, an approach was made to add microalloying elements to a metal-cored wire to strengthen the weld metal [4]. This approach showed promising results, and the outcomes of further experiments with vanadium alloying are discussed elsewhere [5]. Based on these investigations, the strengthening effect of vanadium was incorporated in the alloying concept of this study. Of course, the trade-off between strength and toughness cannot be neglected, particularly in the field of welding of high-strength steels, where thermomechanical processing or heat treatments are inefficient or unwanted. Therefore, the main topic of this paper will be the influence of several alloying elements on the microstructure and consequently the toughness of the investigated weld metal.

A few studies on the influence of different alloying elements on the mechanical properties of high-strength weld metal have been performed in the last decades [6–12]. A comprehensive survey was performed by Keehan et al. who considered several influences on the mechanical behavior of steel welds produced by shielded metal arc welding with a strength in the range of 800–1000 MPa. They varied the contents of carbon, nickel and manganese and correlated the contents to strength and toughness [6–8]. The correlation was based on microstructural investigations, which showed the existence of a mixture of upper and lower bainite, coalesced bainite and martensite [9]. Additionally, an optimum cooling time between 800 and 500 °C of about 3–13 s was determined [10]. In this range a fine microstructure was observed, which was predominantly made responsible for the good strength and toughness. Also other groups investigated the microstructure of this class of material and found the same mixture of bainite and martensite with similar conclusions [11, 12].

However, the desired strength level for the consumable in the current paper requires a fully martensitic microstructure also in the weld metal. A proper way to characterize martensitic all-weld metal was reported in [13] and [14]. The strength and toughness of martensite and the most probable crack propagation paths have been discussed intensely in the last few years by interpreting electron backscatter diffraction (EBSD) results and fracture surfaces. On the one hand, it was concluded that block boundaries are effective grain boundaries for the strengthening of martensite because they hinder dislocation movement [15–17]. On the other hand, the issue of toughness was addressed from several points of view. The fracture path of cleavage crack experiments was investigated in several studies [17–22]. From these studies, one can summarize that cracks can propagate through sub-block boundaries, but not through block boundaries. Therefore, the block size can be interpreted as the effective grain size for toughness and should be small to maximize crack deflection. The misorientation angle chosen for the effective grain size should be about 15°, as the misorientation between sub-blocks is in the range of 5–11° [16, 18].

One further important influence regarding the toughness of steel is the prior austenite grain size (PAGS). High-strength weld metals in the as-welded condition usually exhibit a columnar PAG structure due to the temperature gradient existing [23–25]. The width of the PAG columns depends on the solidification path—which depends on the chemical composition of the liquid weld pool [25]—and the amount of existing inclusions [24]. In high-strength steel weld metal, the width of the PAG columns was associated with the amount of acicular ferrite. Large PAGs promoted the formation of acicular ferrite which is beneficial for toughness [26, 27]. Contrarily, in martensitic steels a small PAGS is generally thought to promote a high toughness. The block size is linearly dependent on the PAGS [28–30]. Therefore, a small PAGS will lead to a small block size, increasing the toughness of the material.

As a consequence, this paper will focus on the evaluation of the effective grain size and its correlation with toughness in martensitic all-weld metal samples. The PAG structure will be investigated regarding its influence on the block size. Grain size variations depending on the chemical composition of the weld metal will be addressed.

Furthermore, an optimized alloying concept will be presented for a new welding consumable with increased strength and adequate toughness.

Materials and methods

The study was carried out on all-weld metal samples which were fabricated according to DIN EN ISO 15792-1 by gas metal arc welding with metal-cored

wires. These samples are built up by seven layers with three weld beads in each layer (Fig. 1). This weld metal design eliminates any influence of the base material on the chemical composition of the weld by dilution and is used to characterize the welding consumable itself. The $t_{8/5}$ cooling time for this kind of sample was measured with thermocouples and is about 5 s for the used set of welding parameters in Table 1.

The chemical composition of the investigated alloys was measured by optical emission spectroscopy and is stated in Table 2. The approximate oxygen content is between 400 and 500 ppm for all samples. Alloy A generally contains the highest amount of alloying elements. Compared to alloy B particularly the carbon content is increased. The main difference between alloys A/B and alloys C/D is the reduced silicon and manganese content in the alloys C/D. Alloy D was additionally alloyed with vanadium for strengthening purposes.

One sample for tensile testing with $d = 10$ mm and $l_0 = 50$ mm, and three Charpy V-notch impact testing samples with a cross section of 10×10 mm^2 were machined out of the all-weld metal samples per alloy for determination of the mechanical properties. The V-notch was located in the middle of the all-weld metal according to DIN EN ISO 15792-1.

EBSD was used for the microstructural characterization of the weld metal. The sample was tilted to 70°, and the scanning electron microscope was operated at 30 kV and a specimen current of ca. 10 nA. Other scan parameters can be found in [13]. The EBSD scans were performed on cross-sections of

the welds and covered a large area (magnification from 300× to 800×) to maximize statistics. As a compromise between acquisition time and scan resolution, a step size of 200–300 nm was chosen. The measurements were carried out in the last deposited bead because only there influences from reheating of the material can be ruled out. For evaluation of the effective grain size, a tolerance angle of 15° was used. Based on the crystallographic orientation relationship between martensite and prior austenite, the PAG structure was reconstructed from the large EBSD scans using ARPGE [31]. The orientation relationship documented by Greninger and Troiano [32] yielded the highest reconstruction quality. The PAG column width was evaluated by applying the linear intercept method. The lines were drawn perpendicular to the longitudinal direction of the PAGs.

For characterization of precipitates, atom probe tomography (APT) was carried out. Several tips were prepared electrolytically from random locations within the all-weld metal and were measured in laser mode at a temperature of 60 K with a laser energy of 0.3 nJ and a pulse repetition rate of 250 kHz.

Results

Mechanical testing

The results of the mechanical testing are summarized in Table 3. Regarding tensile strength and yield strength, no clear trend was observed for samples A, B and C. Contrarily, both tensile and yield strength of sample D are significantly higher. Alloys A/B have a lower impact toughness than alloys C/D, especially at − 20 °C.

Toughness improvement and microstructure—alloys A, B, C

At first, the influence of carbon, manganese and silicon on the microstructure of alloys A, B and C was determined. Alloy D is not shown at this point because of its elevated vanadium content and will be presented in "Combination of strength and toughness improvement–alloy D" section. The short cooling time and the alloying content resulted in a fully martensitic microstructure. Figure 2a–c shows inverse pole figure (IPF) + image quality (IQ) maps of locations in the last deposited weld bead of alloys

Figure 1 Macro-etched all-weld metal sample.

5000 μm

Table 1 Applied welding parameters for the all-weld metal sample

Current	Voltage	Welding speed	Heat input per unit length	Interpass temperature	Wire diameter	Contact tip to work distance
250 A	30 V	50 cm min^{-1}	9 kJ cm^{-1}	150 °C	1.2 mm	15–20 mm

Table 2 Chemical composition of the investigated alloys in wt%

	C	Si	Mn	P	S	Cr + Mo + Ni	V	N
Alloy A	0.12	0.81	2.4	0.012	0.009	4.6	0	0.005
Alloy B	0.08	0.74	2.4	0.009	0.009	3.9	0	0.010
Alloy C	0.08	0.46	1.1	0.008	0.010	4.8	0	0.005
Alloy D	0.09	0.52	1.6	0.012	0.009	4.3	0.22	0.010

Table 3 Mechanical properties of the investigated alloys

	R_m (MPa)	$R_{p0.2}$ (MPa)	A_V at RT (J)	A_V at − 20 °C (J)
Alloy A	1121	953	31 ± 7	21 ± 4
Alloy B	1089	1034	51 ± 1	34 ± 2
Alloy C	1054	993	83 ± 2	70 ± 4
Alloy D	1178	1119	50 ± 2	50 ± 2

A, B and C. The typical needle-shaped morphology of martensite can be identified in all three alloys. While the blocks in alloys A/B show mostly parallel arrangements, alloy C comprises a more chaotic arrangement of blocks with large areas with interlocked structures similar to acicular ferrite [26, 33]. Additionally, the blocks seem to be refined in alloys B and C. The optical appearance of these microstructures was quantified by evaluating the effective grain size and the misorientation distribution from several EBSD scans.

In Table 4 these values are compared with the martensite start temperature (Ms) calculated from the formula below [34].

$$
\begin{aligned}
\text{Ms} = {} & 543 - \left(347C - 4C^2\right) - \left(10.4Ni + 0.5Ni^2\right) \\
& - \left(28.8Mn - 0.26Mn^2\right) + \left(9.7Co - 0.2Co^2\right) \\
& - \left(15.5Cr - 0.58Cr^2\right) + \left(4Si - 0.22Si^2\right) \\
& - \left(1.3Mo + 0.3Mo^2\right) + \left(4Ti - 0.38Ti^2\right) \\
& - C(27Ni + 27Mn + 20Co + 15Cr + 35Si \\
& + 12Mo + 90Ti)
\end{aligned}
$$

The effective grain size decreases, and the average misorientation increases with rising Ms. This trend is graphically represented in Fig. 3. Furthermore, Fig. 4 shows the relationship between Ms and impact toughness at room temperature (Av RT) and at − 20 °C (Av – 20 °C). The impact toughness increases with rising Ms. The difference between room temperature and − 20 °C remains nearly constant.

The PAG structure was reconstructed from the EBSD scans with ARPGE, resulting in the images in Fig. 5a–c. Different PAGs are separated by black lines. The columnar nature of the PAGs is clearly visible. Comparing the three alloys, it is evident that the PAGs of alloy A are much coarser than in alloys B and C. The same situation was found at several different locations in the last deposited bead for each alloy. These scans from several locations per alloy were used to evaluate the corresponding PAGS. The determined values for the PAGS are listed in Table 5 together with the effective grain size. A linear relationship between effective grain size and PAGS is evident, with a factor of approx. 0.11. This relationship is discussed in "Discussion" section.

Combination of strength and toughness improvement—alloy D

For strengthening purposes alloy D contained 0.22 wt% vanadium, which increased the corresponding mechanical values significantly. APT with its nearly atomic resolution was used to study signs of clustering or precipitation in the all-weld metal sample.

Primarily the nearest neighbor distributions (NND) of vanadium atoms were used to identify signs of clustering in the alloy. The NNDs in the reconstructed tips were significantly different from the distributions of the randomized data sets. In most cases distinct peaks were visible with a closer distance of nearest neighbors than would be expected
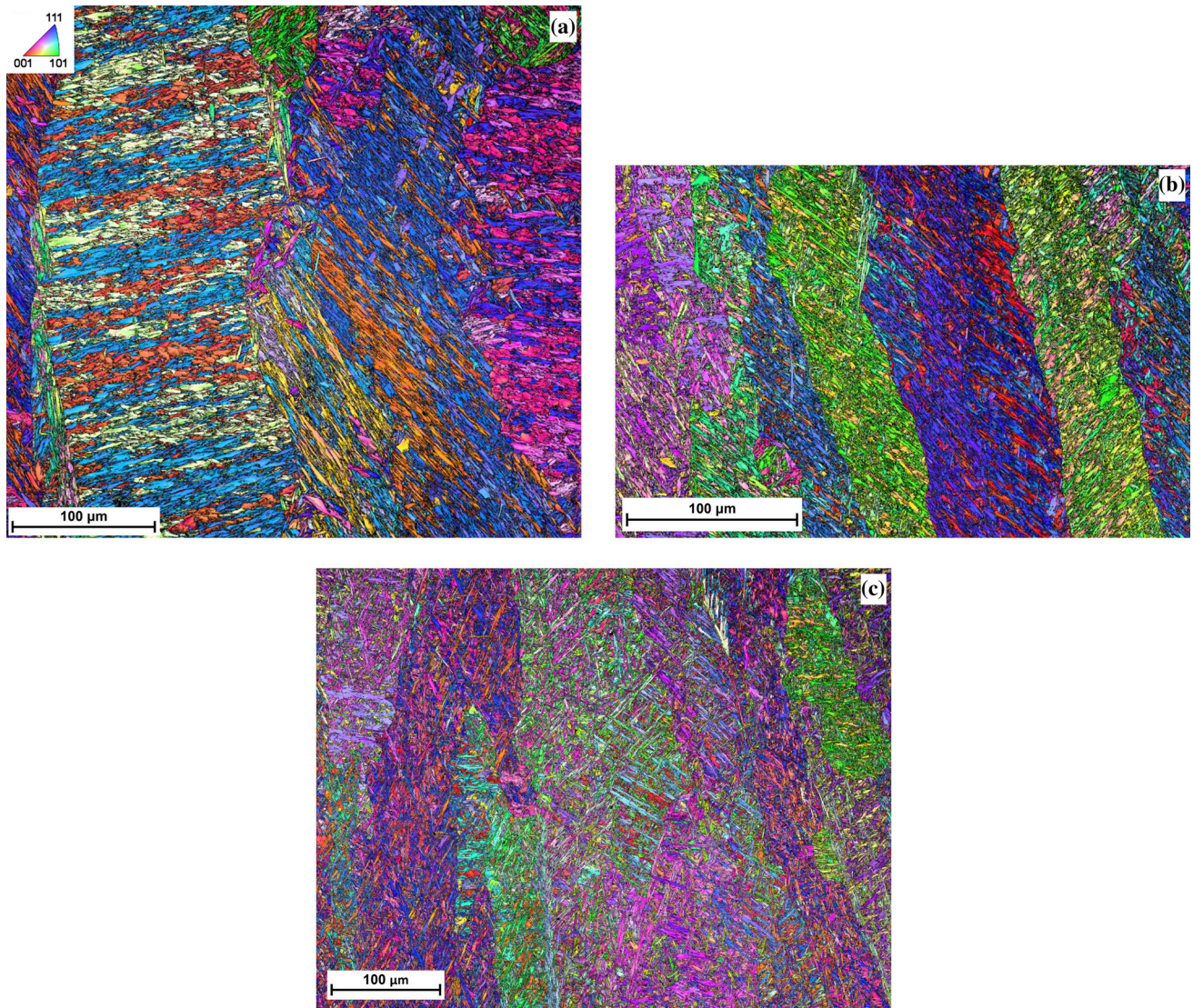
Figure 2 Results from EBSD scans: IPF + IQ maps of locations in the last deposited bead of each alloy. **a** Alloy A, **b** alloy B, **c** alloy C.

Table 4 Comparison of martensite start temperature (Ms) [34] and evaluated effective grain size (EGS) and average misorientation (avM) from EBSD measurements

	Ms (°C)	EGS (μm)	avM (°)
Alloy A	362	8.34 ± 1.28	30.3
Alloy B	397	5.70 ± 1.13	34.4
Alloy C	421	4.59 ± 1.05	38.1

from the randomized data sets. The NND of one reconstruction of a sample of alloy D is depicted in Fig. 6. The peak at 1 nm is a clear sign for clustering of vanadium atoms. Furthermore, the clusters were visualized by isoconcentration surfaces with a concentration value of 2 at.% (Fig. 7a), 4 at.% (Fig. 7b) and 10 at.% (Fig. 7c). The clusters were only visible at small concentration values, contained mostly vanadium, carbon and nitrogen and were still very rich in iron.

The microstructure of alloy D was also investigated with EBSD (Fig. 8) to verify the microstructural changes due to the manganese and silicon content reduction. The martensitic structure looked similar to alloy C, which means the martensite blocks were mostly interlocked and refined. The evaluated effective grain size was 3.34 ± 0.18 μm, the average misorientation was 39.7°, and the PAGS was 49 ± 27 μm. These values are discussed in context with the Ms in "Discussion" section.
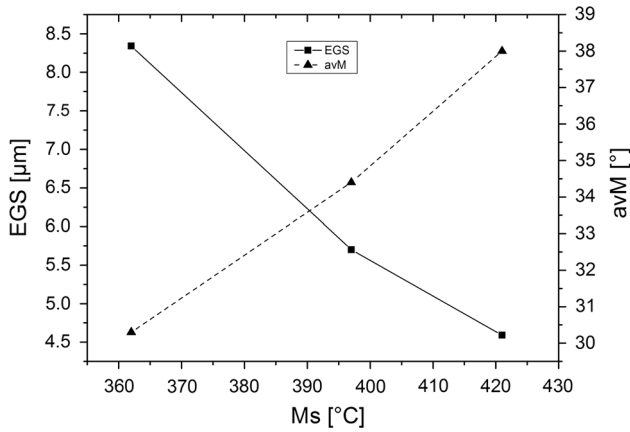
Figure 3 Martensite start temperature (Ms) versus effective grain size (EGS) and average misorientation (avM) of alloys A, B and C.
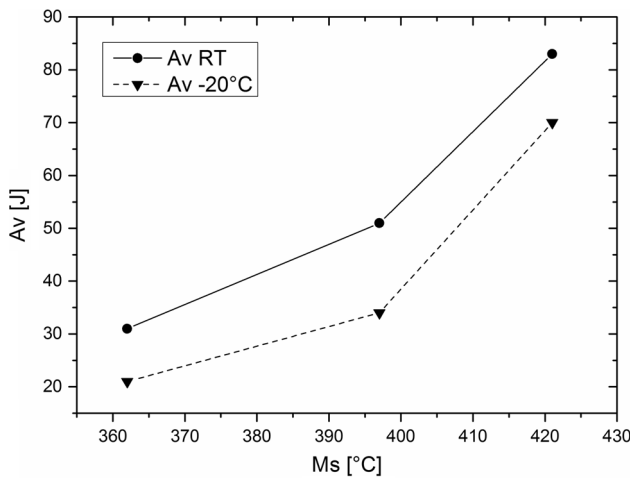
Figure 4 Martensite start temperature (Ms) versus impact toughness at room temperature (Av RT) and at − 20 °C (Av − 20 °C) of alloys A, B and C.

Discussion

The aim of this study was to develop a new generation of welding consumables for welding of high-strength steels. The effects of adjustments in the alloying system on the microstructure and the mechanical properties were investigated using EBSD and APT.

Generally, the welding parameters (voltage, current, speed, etc.) have great influence on the resulting weld [35]. For example, they govern heat input and cooling time, dilution and geometry of the weld. However, when keeping the welding parameters constant, the chemical composition of the weld is the

main influence on the microstructure and therefore the mechanical properties of all-weld metal samples.

Starting from a high-strength steel welding consumable with a guaranteed yield strength of 960 MPa the contents of carbon, manganese and silicon were varied to study their influence on the martensitic microstructure. A decrease in carbon content from 0.12 wt% in alloy A to 0.08 wt% in alloy B influenced the mechanical properties positively. The tensile strength was decreased, but both yield strength and impact toughness were increased. The optical appearance of the microstructure of the different alloys already indicated that alloy C had a refined structure with a more chaotic arrangement of the martensitic blocks (Fig. 2c). This appearance was verified by showing that alloy C had a smaller effective grain size (4.59 μm) and a higher average misorientation (38.1°) than alloys A and B (Table 4). This higher amount of high angle boundaries and smaller size of martensitic blocks implies a higher probability for crack deviation and therefore a higher toughness of the material [18, 21], which was confirmed in the current study.

The linear relationship between block size and PAGS in martensitic microstructures [28–30] was checked by reconstructing the EBSD scans with ARPGE and determining the column width of the PAGS with the linear intercept method. This column width was compared with the effective grain size, which is slightly higher than the block size of martensitic samples. The linear relationship was confirmed (Table 5), meaning that the PAGS may govern the effective grain size and therefore the toughness of the material. However, Fig. 3 suggests a linear dependence of the effective grain size on the Ms, meaning that the Ms may be responsible for grain size changes in the material.

In fact, by comparing Ms and PAGS and their relationship (Fig. 9) one can assume that the Ms acts as indicator of the alloying content of the material. Changing the chemical composition of the weld to increase the Ms will result in a decrease of the PAGS and consequently the effective grain size, which will benefit the toughness of the weld. This theory should not be confused with the often reported phenomenon that the Ms depends on the PAGS [30, 36–39], because that relationship is only valid for chemically identical materials with different PAGSs varied by different austenitization temperatures. The reasons for the dependency of the PAGS on the chemical
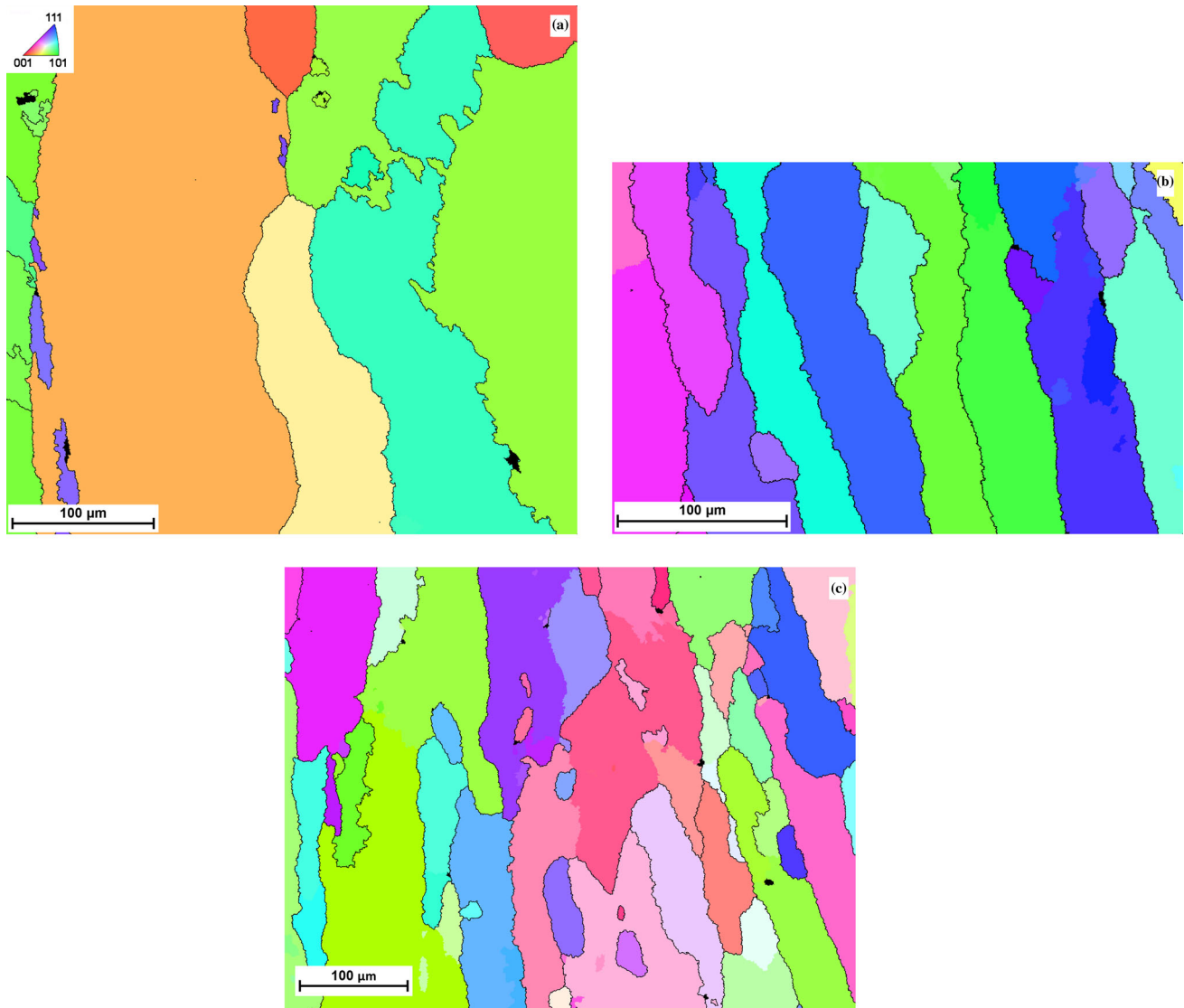
Figure 5 IPF maps of the PAG reconstructions of the scans in Fig. 2. **a** Alloy A, **b** alloy B, **c** alloy C.

Table 5 Evaluated PAGS of alloys A–C with comparison to effective grain size (EGS)

	PAGS (μm)	EGS (μm)
Alloy A	75 ± 50	8.34 ± 1.28
Alloy B	50 ± 29	5.70 ± 1.13
Alloy C	43 ± 22	4.59 ± 1.05

composition of the weld are unclear and should be investigated. Also the reasons for the change from a more parallel arrangement of the martensitic blocks in alloys A and B to a more chaotic arrangement in alloy C are not identified yet and could be subject of further investigations.

Nevertheless, these beneficial changes in microstructure due to a lower manganese and silicon content were applied to the newly developed welding consumable to optimize the toughness.

An addition of vanadium can be used to strengthen the all-weld metal sample in the as-welded condition. In other applications the addition of vanadium is typically lower than 0.1 wt% (vanadium is a well-known microalloying element) [40]. However, in the investigated type of welded material an addition of min. 0.2 wt% vanadium is necessary to attain significant strengthening [5]. Due to the welding process, the material is reheated very shortly by subsequent welding passes. During this short time small clusters

can form, if the vanadium concentration is high enough to guarantee a high clustering potential. Compared to other microalloying elements (Ti, Nb, Al), which were also tried in previous studies [4], vanadium showed the highest strengthening potential and was therefore chosen for this new generation of welding consumables. APT revealed small iron-rich vanadium carbonitride clusters in alloy D (Fig. 7) which increase the strength of the weld.

Alloy D combines the discussed concepts for strengthening and toughening of the welding
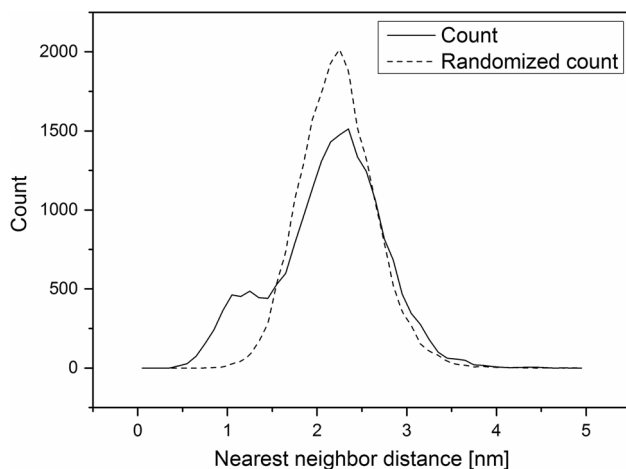
Figure 6 Nearest neighbor distribution of vanadium in an APT sample of alloy D. The peak at about 1 nm distance is a clear sign for clustering of vanadium atoms.

consumable. For reference the microstructure parameters and impact toughness of alloy D are added to Figs. 3 and 4 in Figs. 10 and 11, respectively. Compared to the other alloys, alloy D had the lowest effective grain size and the highest average misorientation and therefore does not fit in the general trend (Fig. 10). Presumably, vanadium also plays a role in refining the martensitic block structure. He and Edmonds [41] proposed a mechanism in bainitic steels that vanadium-rich regions in the PAG promote intragranular nucleation of the ferrite plates, leading to the well-known acicular ferrite structure with a smaller grain size and a superior toughness compared to bainitic structures. A similar mechanism could be responsible for the refinement of the martensitic structure in alloy D of the current study. Nevertheless, this additional grain refinement can only act positively on the mechanical properties and counteracts the toughness loss from the vanadium cluster formation. The resulting toughness (Fig. 11) is in an acceptable range. Particularly, the impact toughness at -20 °C does not seem to suffer from the vanadium cluster formation and fulfills the requirement of 47 J at -20 °C.

Overall, the combination of increasing the Ms by reducing the manganese and silicon content and adding vanadium to induce cluster formation resulted in a possible new generation of high-strength steel welding consumables with an increased strength and adequate toughness.
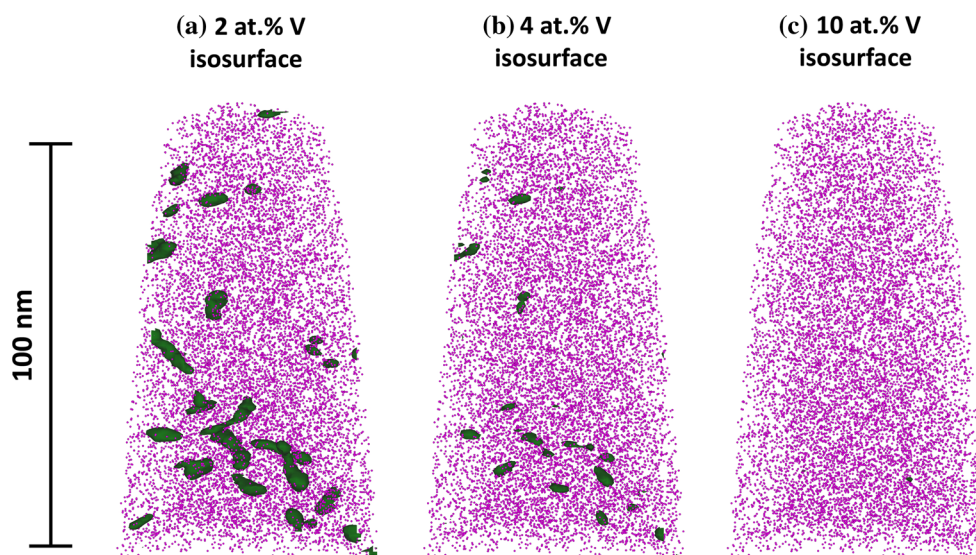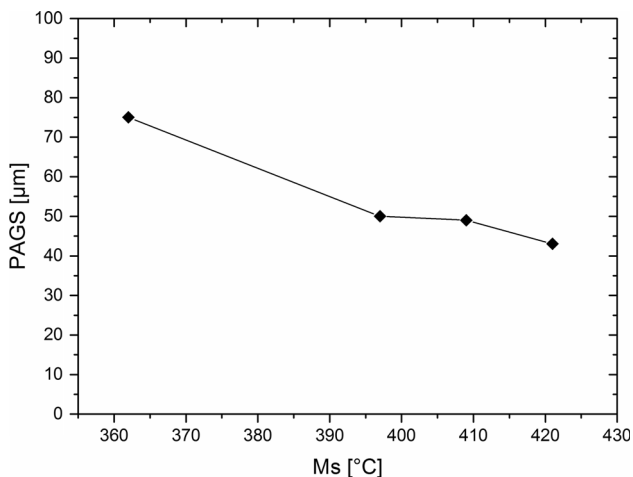

Figure 7 Reconstructed tip of an atom probe measurement of alloy D. The pink dots represent the iron matrix of the alloy. Vanadium isoconcentration surfaces with concentration values of **a** 2 at.%, **b** 4 at.% and **c** 10 at.% visualize the existence of vanadium-rich clusters.
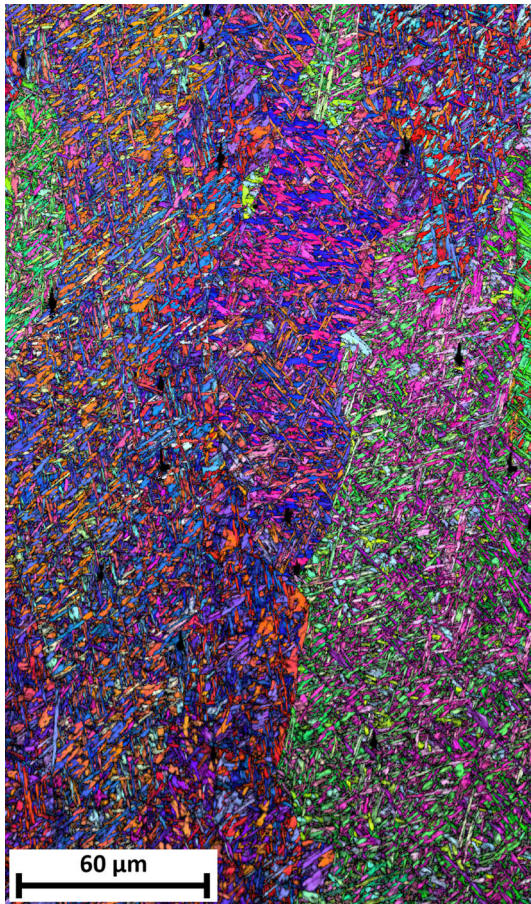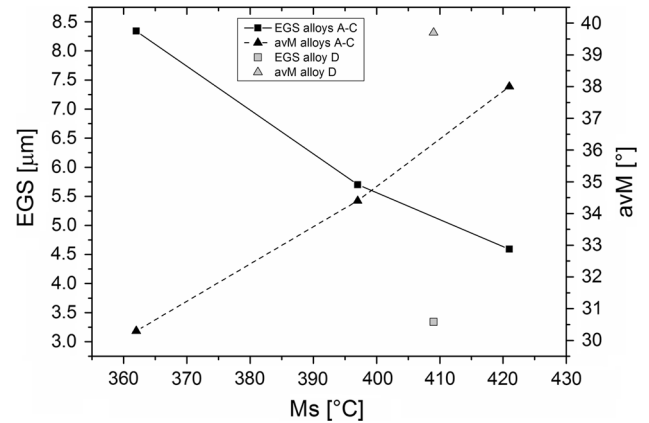
Figure 8 Result from EBSD scan: IPF + IQ map of location in the last deposited bead of alloy D.
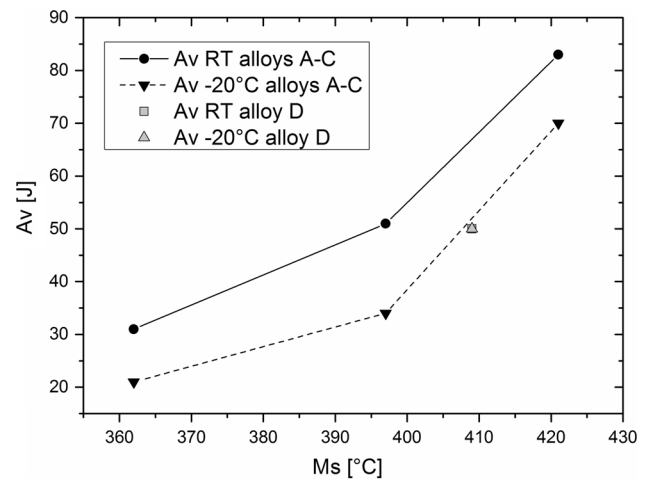

Figure 9 Martensite start temperature (Ms) versus prior austenite grain size (PAGS) of alloys A, B, C and D.

The fatigue performance of this welding consumable was not investigated so far. In the last few years the concept of low transformation temperature (LTT)

Figure 10 Martensite start temperature (Ms) versus effective grain size (EGS) and average misorientation (avM) of alloys A, B, C and D.

Figure 11 Martensite start temperature (Ms) versus impact toughness at room temperature (Av RT) and at − 20 °C (Av − 20 °C) of alloys A, B and C.

filler wires emerged for welding of ultra-high-strength steels because of the resulting compressive residual stresses and low welding distortion, which act positively on the fatigue strength [42–44]. From that point of view, the current study with its suggestion to increase the Ms worked in the opposite direction, and the resulting weld will probably have tensile residual stresses [42]. However, despite its much lower alloying content, the static strength of the current material is much higher than the static strength of LTT wires. Also, LTT wires typically contain high amounts of nickel and chromium, which makes them quite costly compared to the proposed low alloy filler wire. Consequently, the fatigue

performance of the current material should be a focus of following studies.

In the intended applications the high-strength steel welds are usually deployed in the as-welded condition. That is also recommended for the current welding consumable, as the high vanadium content might induce severe precipitate formation and possibly deterioration of toughness after a post weld heat treatment.

Conclusions

A new generation of welding consumables for high-strength steels was developed by changing the alloying contents of carbon, manganese, silicon and vanadium. The produced all-weld metal samples were characterized regarding their microstructure with EBSD and APT. The relationship between microstructure and mechanical properties was determined and directly applied to the new welding consumable. The following conclusions can be drawn from the investigations:

- Lowering the manganese and silicon content and consequently increasing the martensite start temperature resulted in a lower prior austenite grain size and effective grain size and a higher average grain boundary misorientation of the martensitic microstructure. These microstructural changes improved the impact toughness of the weld metal.
- Vanadium alloying strengthened the weld metal significantly due to the formation of vanadium-rich clusters. Furthermore, an additional refinement of the martensitic microstructure due to the vanadium alloying was observed.
- A combination of the toughening concept and the strengthening concept was used to produce an all-weld metal sample with a strength of more than 1100 MPa while keeping the impact toughness above 47 J at room temperature and at $-20\ °C$.

Acknowledgements

Compliance with ethical standards

Conflict of interest The authors declare that they have no conflict of interest.

References

[1] Khurshid M, Barsoum Z, Mumtaz NA (2012) Ultimate strength and failure modes for fillet welds in high strength steels. Mater Des 40:36–42. https://doi.org/10.1016/j.matdes.2012.03.048

[2] Lan L, Kong X, Qiu C, Zhao D (2016) Influence of microstructural aspects on impact toughness of multi-pass submerged arc welded HSLA steel joints. Mater Des 90:488–498. https://doi.org/10.1016/j.matdes.2015.10.158

[3] Schneider C, Ernst W, Schnitzer R, et al (2018) Welding of S960MC with undermatching filler material. Submitted to Weld World

[4] Schnitzer R, Zügner D, Haslberger P et al (2017) Influence of alloying elements on the mechanical properties of high-strength weld metal. Sci Technol Weld Join 22:536–543. https://doi.org/10.1080/13621718.2016.1274095

[5] Haslberger P, Holly S, Ernst W, Schnitzer R (2018) Precipitates in microalloyed ultra-high strength weld metal studied by atom probe tomography. Submitted to Weld World

[6] Keehan E, Karlsson L, Andrén H-O (2006) Influence of carbon, manganese and nickel on microstructure and properties of strong steel weld metals, Part 1—effect of nickel content. Sci Technol Weld Join 11:1–8

[7] Keehan E, Karlsson L, Andrén H-O, Bhadeshia HKDH (2006) Influence of carbon, manganese and nickel on microstructure and properties of strong steel weld metals, Part 2—impact toughness gain resulting from manganese reductions. Sci Technol Weld Join 11:9–18

[8] Keehan E, Karlsson L, Andrén H-O, Bhadeshia HKDH (2006) Influence of carbon, manganese and nickel on microstructure and properties of strong steel weld metals,

Part 3—increased strength resulting from carbon additions. Sci Technol Weld Join 11:19–24

[9] Keehan E, Karlsson L, Thuvander M, Bergquist E (2007) Microstructural characterisation of as-deposited and reheated weld metal—high strength steel weld metals. Weld World 51:44–49. https://doi.org/10.1007/BF03266559

[10] Keehan E, Zachrisson J, Karlsson L (2010) Influence of cooling rate on microstructure and properties of high strength steel weld metal. Sci Technol Weld Join 15:233–238. https://doi.org/10.1179/136217110X12665048207692

[11] Wansheng D, Yun P, Hongjun X et al (2010) Microstructure and toughness of 1000 MPa high strength weld metal. Mater Sci Forum 638–642:3441–3446

[12] Zhang T, Li Z, Ma S et al (2016) High strength steel (600–900 MPa) deposited metals: microstructure and mechanical properties. Sci Technol Weld Join 21:186–193. https://doi.org/10.1179/1362171815Y.0000000079

[13] Haslberger P, Ernst W, Schnitzer R (2017) High resolution imaging of martensitic all-weld metal. Sci Technol Weld Join 22:336–342. https://doi.org/10.1080/13621718.2016.1240980

[14] Haslberger P, Holly S, Ernst W, Schnitzer R (2017) Microstructural characterization of martensitic all-weld metal samples. Pract Metallogr 54:513–532. https://doi.org/10.3139/147.110464

[15] Shibata A, Nagoshi T, Sone M et al (2010) Evaluation of the block boundary and sub-block boundary strengths of ferrous lath martensite using a micro-bending test. Mater Sci Eng A 527:7538–7544. https://doi.org/10.1016/j.msea.2010.08.026

[16] Mine Y, Hirashita K, Takashima H et al (2013) Micro-tension behaviour of lath martensite structures of carbon steel. Mater Sci Eng A 560:535–544. https://doi.org/10.1016/j.msea.2012.09.099

[17] Du C, Hoefnagels JPM, Vaes R, Geers MGD (2016) Block and sub-block boundary strengthening in lath martensite. Scr Mater 116:117–121. https://doi.org/10.1016/j.scriptamat.2016.01.043

[18] Kim M-C, Jun OhY, Hwa Hong J (2000) Characterization of boundaries and determination of effective grain size in Mn-Mo-Ni low alloy steel from the view of misorientation. Scr Mater 43:205–211. https://doi.org/10.1016/S1359-6462(00)00392-4

[19] Gourgues A-F, Flower HM, Lindley TC (2000) Electron backscattering diffraction study of acicular ferrite, bainite, and martensite steel microstructures. Mater Sci Technol 16:26–40. https://doi.org/10.1179/026708300773002636

[20] Wang C, Wang M, Shi J et al (2007) Effect of microstructure refinement on the strength and toughness of low alloy martensitic steel. J Mater Sci Technol 23:659–664

[21] Morris JW, Kinney C, Pytlewski K, Adachi Y (2013) Microstructure and cleavage in lath martensitic steels. Sci Technol Adv Mater 14:14208. https://doi.org/10.1088/1468-6996/14/1/014208

[22] Wu Q, Zikry MA (2014) Microstructural modeling of crack nucleation and propagation in high strength martensitic steels. Int J Solids Struct 51:4345–4356. https://doi.org/10.1016/j.ijsolstr.2014.08.021

[23] Bhadeshia HKDH, Svensson LE, Gretoft B (1986) The austenite grain structure of low-alloy steel weld deposits. J Mater Sci 21:3947–3951. https://doi.org/10.1007/BF00553451

[24] Grong O, Matlock DK (1986) Microstructural development in mild and low-alloy steel weld metals. Int Met Rev 31:27–48. https://doi.org/10.1179/imtr.1986.31.1.27

[25] Zhang Z, Farrar RA (1995) Columnar grain development in C-Mn-Ni low-alloy weld metals and the influence of nickel. J Mater Sci 30:5581–5588. https://doi.org/10.1007/BF00356690

[26] Farrar RA, Harrison PL (1987) Acicular ferrite in carbon-manganese weld metals: an overview. J Mater Sci 22:3812–3820. https://doi.org/10.1007/BF01133327

[27] Babu SS, Bhadeshia HKDH (1991) Mechanism for the transition from bainite to acicular ferrite. Mater Trans 32:679–688

[28] Morito S, Saito H, Ogawa T et al (2005) Effect of austenite grain size on the morphology and crystallography of lath martensite in low carbon steels. ISIJ Int 45:91–94. https://doi.org/10.2355/isijinternational.45.91

[29] Galindo-Nava EI, Rivera-Díaz-del-Castillo PEJ (2015) A model for the microstructure behaviour and strength evolution in lath martensite. Acta Mater 98:81–93. https://doi.org/10.1016/j.actamat.2015.07.018

[30] Hidalgo J, Santofimia MJ (2016) Effect of prior austenite grain size refinement by thermal cycling on the microstructural features of as-quenched lath martensite. Metall Mater Trans A Phys Metall Mater Sci 47:1–14. https://doi.org/10.1007/s11661-016-3525-4

[31] Cayron C (2007) ARPGE: a computer program to automatically reconstruct the parent grains from electron backscatter diffraction data. J Appl Crystallogr 40:1183–1188. https://doi.org/10.1107/S0021889807048777

[32] Greninger AB, Troiano AR (1949) The mechanism of martensite formation. Trans AIME 185:590–598

[33] Wan XL, Wang HH, Cheng L, Wu KM (2012) The formation mechanisms of interlocked microstructures in low-carbon high-strength steel weld metals. Mater Charact 67:41–51. https://doi.org/10.1016/j.matchar.2012.02.007

[34] Galindo-Nava EI (2017) On the prediction of martensite formation in metals. Scr Mater 138:6–11. https://doi.org/10.1016/j.scriptamat.2017.05.026

[35] Messler RW (1999) Principles of welding. Wiley, Weinheim. https://doi.org/10.1002/9783527617487

[36] Brofman PJ, Ansell GS (1983) On the effect of fine grain size on the Ms temperature in Fe-27Ni-0.025C alloys. Metall Trans A 14:1929–1931. https://doi.org/10.1007/BF02645565

[37] Guimarães JRC, Rios PR (2010) Martensite start temperature and the austenite grain-size. J Mater Sci 45:1074–1077. https://doi.org/10.1007/s10853-009-4044-0

[38] García-Junceda A, Capdevila C, Caballero FG, de Andrés CG (2008) Dependence of martensite start temperature on fine austenite grain size. Scr Mater 58:134–137. https://doi.org/10.1016/j.scriptamat.2007.09.017

[39] van Bohemen SMC, Morsdorf L (2017) Predicting the Ms temperature of steels with a thermodynamic based model including the effect of the prior austenite grain size. Acta Mater 125:401–415. https://doi.org/10.1016/j.actamat.2016.12.029

[40] Lagneborg R, Siwecki T, Zajac S, Hutchinson B (1999) The role of vanadium in microalloyed steels. Scand J Metall 28(5):186–241

[41] He K, Edmonds DV (2002) Formation of acicular ferrite and influence of vanadium alloying. Mater Sci Technol 18:289–296. https://doi.org/10.1179/026708301225000743

[42] Francis JA, Stone HJ, Kundu S et al (2009) The effects of filler metal transformation temperature on residual stresses in a high strength steel weld. J Press Vessel Technol 131:41401. https://doi.org/10.1115/1.3122036

[43] Ooi SW, Garnham JE, Ramjaun TI (2014) Review: low transformation temperature weld filler for tensile residual stress reduction. Mater Des 56:773–781. https://doi.org/10.1016/j.matdes.2013.11.050

[44] Harati E, Karlsson L, Svensson LE, Dalaei K (2017) Applicability of low transformation temperature welding consumables to increase fatigue strength of welded high strength steels. Int J Fatigue 97:39–47. https://doi.org/10.1016/j.ijfatigue.2016.12.007

Springer